

Supporting Information

N-Alkyl substituted triazenide-bridged homoleptic iron(II) dimers with an exceptionally short Fe–Fe bond

Khaled Soussi^a, Erwann Jeanneau^b, Pascale Maldivi^c, Martin Clémancey^d, Jean-Marc Latour^d, Lhoussain Khrouz^e, Chantal Lorentz^a, Stéphane Daniele^{f} and Shashank Mishra^{a*}*

^a Université Claude Bernard Lyon 1, CNRS, UMR 5256, Institut de Recherches sur la Catalyse et l'Environnement de Lyon (IRCELYON), 2 av. Albert Einstein, 69626 Villeurbanne, France. E-mail : shashank.mishra@ircelyon.univ-lyon1.fr; Fax: 33-472445399; Tel: 33 472445360.

^b Université Claude Bernard Lyon 1, Centre de Diffractométrie Henri Longchambon, 5 rue de La Doua, 69100 Villeurbanne, France.

^c Univ. Grenoble Alpes, CEA, CNRS, IRIG, DIESE, LCBM, pmb, F-38000 Grenoble, France.

^d Univ. Grenoble Alpes, CEA, CNRS, IRIG, DIESE, SyMMES, F-38000 Grenoble, France.

^e Université de Lyon, ENS de Lyon, CNRS, Université Lyon 1, Laboratoire de Chimie, F69342, Lyon, France.

^f Université Claude Bernard Lyon 1, CNRS-UMR 5218, CP2M-ESCEPE Lyon, 43 Bd du 11 Nov. 1918, 69616 Villeurbanne, France. E-mail : stephane.daniele@univ-lyon1.fr

Experimental

General Procedures. All other manipulations were performed under the argon atmosphere using standard Schlenk and glovebox techniques. Solvents were distilled using MB SPS-800 and were used without further purification. New triazine ligands HN_3^tBuR ($\text{R} = \text{Et}, ^i\text{Pr}, ^n\text{Bu}$) featuring different alkyl substituents at 1,3-N centers ligands were prepared as reported in our earlier report.¹ $\text{Fe}[\text{N}(\text{SiMe}_3)_2]_2$ was synthesized according to the published procedure.² The infrared spectra were obtained as Nujol mulls on a Bruker Vector 22 FT-IR spectrometer at room temperature and registered from 4000 to 400 cm^{-1} . Thermogravimetric analyses (TGA) were performed with a TGA/DSC 1 STARe System from Mettler Toledo. Around 8 mg of the sample were sealed in a 100 ml Al crucible in the glovebox and heated under argon atmosphere at a heating rate of 5 $^\circ\text{C}/\text{min}$. Fitting of the curves was done using origin software. ^{57}Fe Mössbauer spectra were recorded on powder samples contained in Delrin cups at 5 K on a strong-field Mössbauer spectrometer equipped with an Oxford Instruments Spectromag 4000 cryostat containing an 8 T split-pair superconducting magnet. The spectrometer was operated in a constant acceleration mode in transmission geometry. The isomer shifts were referenced against that of a room-temperature metallic iron foil. Analysis of the data was performed with the WMOSS Mössbauer Spectral Analysis Software (www.wmoss.org, 2012–2013, Web Research, Edina) and with a home-made program (SimuMoss software. C. Charavay, S. Segard, F. Edon, M. Clémancey, G. Blondin. CEA/iRTSV, CNRS, Univ. Grenoble Alpes).³ EPR assays were all carried out at helium temperatures using a Bruker EMX spectrometer operating at X-band with double cavity. The instrument settings were as follows: 100 kHz modulation frequency, 6.5-22mW microwave power, 5 G modulation amplitude. The wide range ^1H NMR spectra of Fe(II) complexes in the range -150 ppm to 500 ppm were recorded in CDCl_3 on AVANCE HD 400 spectrometer operating at 400.13 MHz. Samples for magnetic susceptibility measurements using the Evans method were prepared by dissolving a weighed

amount of the iron(II) complex **3** in a measured amount of a deuterated chloroform solvent. The solution was transferred into a 5 mm NMR tube containing a 1 mm capillary with the deuterated chloroform as a reference. The peak separation of the solvent resonance between that of pure solvent (in the capillary) and that shifted by the paramagnetic solution (outside of the capillary) was used for determining the susceptibility in solution.

Computational details

All calculations were done in the framework of Density Functional Theory (DFT) using ADF 2018^{4,5} on complex **1**. Geometry optimizations were carried out with OLYP as a pure GGA or B3LYP as a hybrid functional, and dispersion terms were included through the Grimme3 correction. A TZ2P basis set was used throughout all calculations, with a small core for OLYP calculations and all electrons for B3LYP ones. Default integration and grid accuracy parameters were used. Open-shell singlet calculations were run either by imposing initial spin densities on the Fe atoms potential with MODIFYSTARTPOTENTIAL or by using the standard broken symmetry approach with spin flipping. The final spin densities were then controlled after each calculation. Indeed, single points on the X-ray structures with singlet calculations always converged to local null spin projections whatever the starting conditions. Geometry optimizations allowed to reach some other low-lying configurations depending on initial conditions. Mössbauer parameters were calculated following an already reported protocol⁶ with B3LYP and the TZ2P basis set. The hyperfine coupling tensor components were calculated⁷ from the B3LYP optimized geometry in triplet state. ADF 2018 was used with the scalar ZORA Hamiltonian⁸ and ZORA-QZ4P all electron basis sets for Fe and N atoms, the rest being treated with TZ2P all electron ZORA basis sets. The spin-orbit ZORA Hamiltonian either did not converge or converged to non-consistent A values, which can be explained by the impossibility to impose a spin-only value within a two-component approach and by the existence of other low-lying spin states values. We also employed Orca 4.2^{9,10} with the scalar ZORA approach

and the spin-orbit perturbation method, together with ZORA adapted def2-tzvp basis set, the uncontracted core-properties CP(PPP) basis set for Fe and IGLO-II for N atoms together with an increased grid accuracy of 6. The RIJCOSX approximation was employed to speed up the calculations of Coulomb and exchange integrals. The spin-orbit coupling was taken into account through the mean-field / effective nuclear charge approach with 1-electron terms.

Synthesis of new iron(II) triazenide complexes

[Fe₂(N₃^tBuEt)₄] (1). To a pre-stirred solution of Fe[N(SiMe₃)₂]₂ (0.89g, 2.36 mmol) in *n*-hexane was added 0.67 g (4.72 mmol) of HN₃^tBuEt at 0 °C and then the temperature was allowed to increase gradually to room temperature. The dark brown mixture obtained was stirred for 18 h, after which the volatile materials were removed under vacuum. Brown crystals of the complex were obtained by crystallization in anhydrous hexane at -20 °C. Yield, 0.79 g (54%). Anal.: Calcd for C₂₄H₅₆N₁₂Fe₂ (624.5): C 46.12, H 8.96, N 26.90; found C 46.21, H 9.06, N 26.82%. FT-IR (Nujol, cm⁻¹): 1678w, 1516m, 1461m, 1375m, 1305m, 1203w, 1078w, 1017w, 972w.

Using above method, complexes **2** and **3** were also synthesized from the reactants given below in the parentheses and purified by crystallization in anhydrous hexane at -20 °C.

[Fe₂(N₃^tBuⁱPr)₄] (2). Fe[N(SiMe₃)₂]₂ (0.86 g, 2.47 mmol) and HN₃^tBuⁱPr (0.78 g, 4.95 mmol) in anhydrous hexane. Yield, 1.12 g (67%). Anal.: calcd for C₂₈H₅₈N₁₂Fe₂ (674.5): C 49.81, H 8.59, N 24.90; found C 49.93, H 8.68, N 24.82%. FT-IR (Nujol, cm⁻¹): 1451m, 1355m, 1241s, 1200m, 1108m, 1032m, 992s, 840s, 674m, 613w, 553w.

[Fe₂(N₃^tBuⁿBu)₄] (3). Fe[N(SiMe₃)₂]₂ (0.83 g, 2.21 mmol) and HN₃^tBuⁿBu (0.57 g, 5.17 mmol) in anhydrous hexane. Yield, 1.60 g (61%). Anal.: calcd for C₃₂H₆₀N₁₂Fe₂ (724.6): C 52.99, H 8.28, N 28.13; found C 53.09, H 8.19, N 28.03%. FT-IR (Nujol, cm⁻¹): 1673w, 1512m, 1456s, 1388s, 1300m, 1265m, 1209m, 1027w, 734w, 660w, 580w.

X-ray crystallography: Crystal structures of the **1** and **3** were measured using Mo radiation ($\lambda = 0.71073 \text{ \AA}$) on an Oxford Diffraction Gemini diffractometer equipped with an Atlas CCD detector. Intensities were collected at 150 K (for **1**) or 100 K (for **3**) by means of the CrysAlisPro software.¹¹ Reflection indexing, unit-cell parameters refinement, Lorentz-polarization correction, peak integration and background determination were carried out with the CrysAlisPro software.¹¹ An analytical absorption correction was applied using the modeled faces of the crystal.¹² The resulting sets of hkl were used for structure solutions and refinements. The structures were solved with the ShelXT¹³ structure solution program using the intrinsic phasing solution method and by using Olex2¹⁴ as the graphical interface. The model was refined with version 2018/3 of ShelXL¹⁵ using least-squares minimization.

CCDC 1555083 and 1555084 contain the supplementary crystallographic data for this paper. These data can be obtained free of charge from The Cambridge Crystallographic Data Centre via www.ccdc.cam.ac.uk/data_request/cif.

References

- (1) K. Soussi, S. Mishra, E. Jeanneau, J.-M. M. Millet and S. Daniele, Asymmetrically substituted triazenes as poor electron donor ligands in the precursor chemistry of iron(II) for iron-based metallic and intermetallic nanocrystals, *Dalton Trans.* 2017, 46, 13055–13064.
- (2) R. A. Anderson, K. Faegri, J. C. Green, A. Haaland, M. F. Lappert, W. P. Leung and K. Rypdal, Synthesis of Bis[bis(trimethylsilyl)amido]iron(II). Structure and Bonding in $M[N(\text{SiMe}_3)_2]_2$ (M = Manganese, Iron, Cobalt): Two-coordinate Transition Metal Amides. *Inorg. Chem.* 1988, 27, 1782-1786.

- (3) M. Carboni, M. Clémancey, F. Molton, J. Pécaut, C. Lebrun, L. Dubois, G. Blondin and J.-M. Latour, Biologically Relevant Heterodinuclear Iron–Manganese Complexes. *Inorg. Chem.* 51, 10447–10460 (2012).
- (4) G. Te Velde, F. M. Bickelhaupt, E. J. Baerends, C. Fonseca Guerra, S. J. A. van Gisbergen, J. G. Snijders and T. Ziegler, Chemistry with ADF, *J. Computational Chem.* 2001, 22, 931.
- (5) C. Fonseca Guerra, J. G. Snijders, G. Te Velde and E. J. Baerends, Towards an order-N DFT method, *Theoretical Chem. Acc.* 1998, 99, 391.
- (6) A. Parent, C. Caux-Thang, L. Signor, M. Clémancey, R. Sethu, Ge. Blondin, P. Maldivi, V. Duarte and J.-M. Latour, A single glutamate to aspartate mutation makes Fur sensitive to H₂O₂ as PerR. *Angew. Chem. Int. Ed.* 2013, 52, 10339-43.
- (7) E. van Lenthe, A. van der Avoird and P. E. S. Wormer *J. Chem. Phys.* 1998, 108, 4783.
- (8) E. van Lenthe, E. J. Baerends and J. G. Snijders, Relativistic regular two-component Hamiltonians, *J. Chem. Phys.* 1993, 99, 4597.
- (9) F. Neese, The ORCA program system, *Wiley Interdiscip. Rev.: Comput. Mol. Sci.* 2012, 2, 73-78.
- (10) F. Neese, Software update: the ORCA program system, version 4.0, *Wiley Interdiscip. Rev.: Comput. Mol. Sci.* 2017, 8, e1327.
- (11) CrysAlisPro, Agilent Technologies, Version 1.171.36.28 (release 01-02-2013 CrysAlis171.NET) (compiled Feb 1 2013, 16:14:44).
- (12) R. C. Clark and J. S. Reid, The Analytical Calculation of Absorption in Multifaceted Crystals. *Acta Cryst.* 1995, A51, 887-897.
- (13) G. M. Sheldrick, *Acta Cryst.* 2015, A71, 3-8.
- (14) O.V. Dolomanov, L. J. Bourhis, R. J. Gildea, J. A. K. Howard and H. Puschmann, *J. Appl. Cryst.* 2009, 42, 339-341.
- (15) G. M. Sheldrick, *Acta Cryst.* 2015, C27, 3-8.

Table S1. Crystallographic and refinement data for new Fe(II) triazenide complexes.

Compound	1	3
Empirical formula	C ₂₄ H ₅₆ Fe ₂ N ₁₂	C ₃₂ H ₇₂ Fe ₂ N ₁₂
Formula weight	624.5	736.7
Crystal system	Orthorhombic	Monoclinic
Space group	<i>Pccn</i>	<i>C2/c</i>
a (Å)	12.1992(15)	19.115(2)
b (Å)	12.3984(18)	11.7866(8)
c (Å)	21.399(3)	21.137(2)
α (°)	90	90
β (°)	90	120.907(16)
γ (°)	90	90
V (Å ³)	3236.6(7)	4086.0(9)
Z	4	4
μ (mm ⁻¹)	0.94	0.75
Temperature (K)	150	100
Measured reflections	16252	42383
Independent reflections (R _{int})	4014	5396 (0.068)
Data/restraints/parameters	4014/0/181	5396/0/216
Goodness of fit	1.04	1.11
R[F ² >2σ(F ²)]	0.064	0.055
wR(F ²)	0.190	0.162
Residual electron density (e.Å ⁻³)	-1.20 to 1.54	-0.85 to 0.79
CCDC no.	1555083	1555084

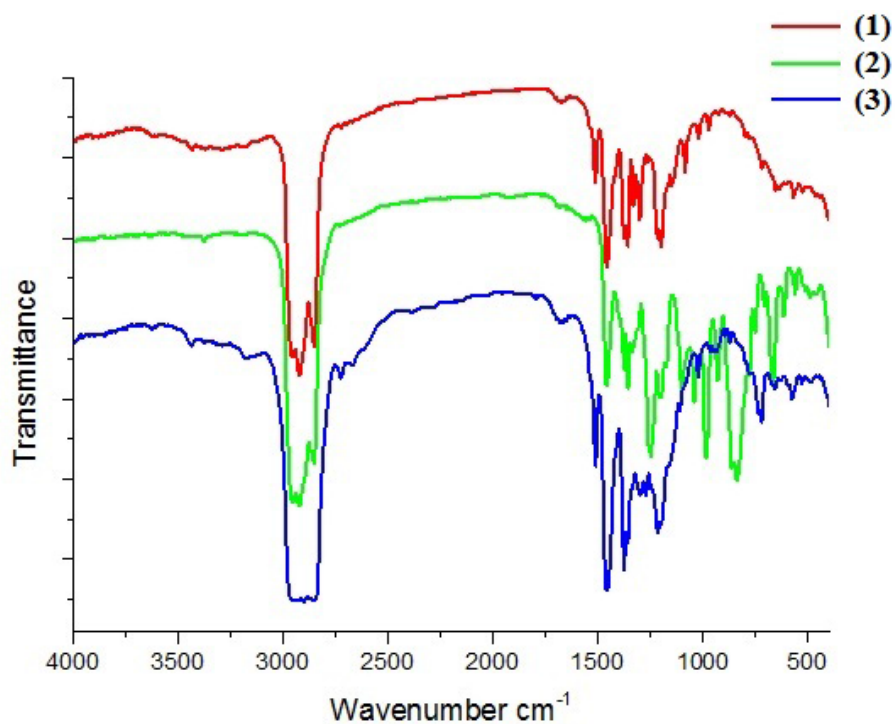


Figure S1: FT-IR spectra of the new Fe(II) complexes **1-3**.

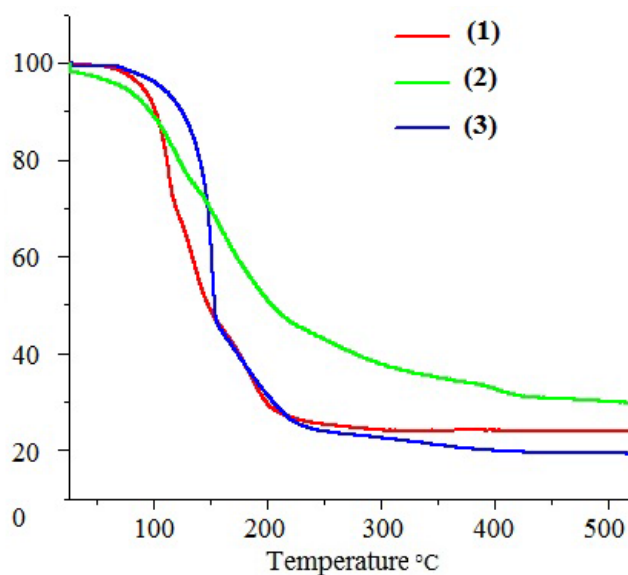


Figure S2. TGA curves of **1-3**.

Even though not very volatile, the TGA curves of these dimeric complexes $[\text{Fe}_2(\text{N}_3\text{-}^i\text{BuR})_4]$ [R = Et (**1**), ^iPr (**2**), ^nBu (**3**)] do indicate gradual loss of the triazine ligands in 2 to 3-decomposition steps with the end residues at 450 °C corresponding mostly to the metallic iron

(e.g., 18% exp vs. 17.9% calcd. for **1** and 15% exp vs. 15.1% calcd. for **3**). This is further supported by the Fe 2p XPS spectrum of **1** decomposed *in-situ* at 500 °C for 2 h, producing about 55% metallic Fe(0) component (Figure S3). The presence of some iron oxide particles during decomposition indicates the high air-sensitivity of this complex.

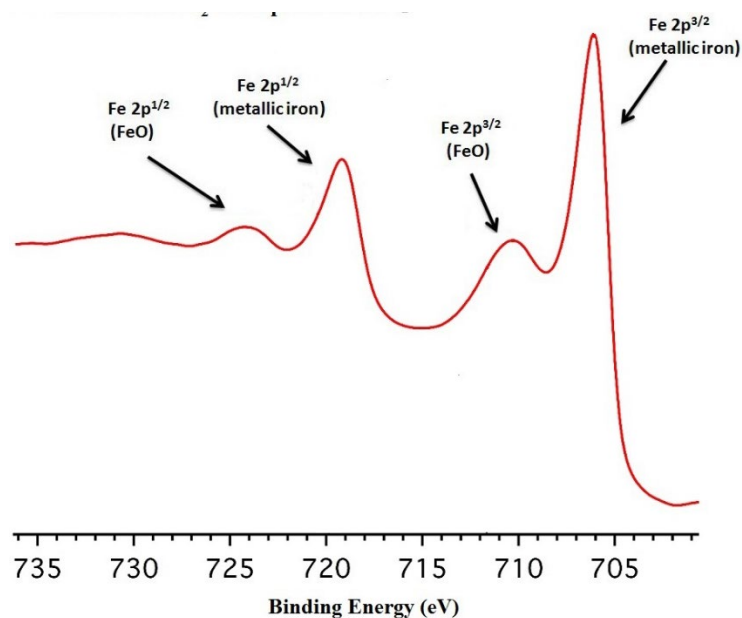


Figure S3. Fe 2p XPS spectrum of the complex **1** decomposed *in situ* at 500°C.

Cyclic voltammetry was performed on **1-3** to understand the electrochemical properties of these complexes. Experiments were conducted under a constant flow of argon gas using a standard three-electrode setup with a glassy carbon working disc electrode and a platinum wire auxiliary electrode and colomel saturated electrode reference electrode. The dimeric complexes **1-3** showed an irreversible oxidation process (Fig. S4a). The voltammograms exhibited highest oxidation potential for the complex with the bulkiest ligand (1.86 V for **3** as compared to 1.78 and 1.73 V for **1** and **2**, respectively). No clear-cut effect of the ligand on the evolution of the oxidation potential was found and the complexes with N₃^tBuⁿBu ligand has the highest oxidation potential.

To understand the electrochemical behavior of the dimers, electrolysis was performed on the representative example [Fe₂(N₃^tBuEt)₄] (**1**) to calculate the number of electrons involved in the oxidation process. It is an electro-analytical process that determines the quantity of electricity (Q in coulomb) experimentally by completely oxidizing or reducing a known quantity of a chemical compound. The working electrode was kept at a constant potential and the current that flows through the circuit was measured. As the electroactive molecules were consumed, the

current also decreased, approaching zero when the conversion was complete. Cyclic voltammetry of **1** was performed before electrolysis experiment in anhydrous dichloromethane in order to assess the potential needed to oxidize these complexes in an electrolysis experiment. Cyclic voltammetry was then performed after electrolysis to verify if all the quantity was consumed (Fig. S4b). The sample mass, molecular mass, number of electrons in the electrode reaction, and number of electrons passed during the experiment are all related by Faraday's laws (eq. 1).

$$Q = mFn e^{-} \quad (1)$$

Where Q = electrical charge, measured experimentally by calculating the area under the curve I (A) vs time (min); m = number of mole of the compound; F = Faraday's constant (96500); and ne^{-} = number of electrons involved in the electrochemical process.

The potential of the working electrode needed to completely oxidize the quantity of a chemical compound in an electrolysis experiment is determined by cyclic voltammetry and it corresponds to the oxidation peak of the compound.

Number of electrons involved in the oxidation of **1** (assuming that the electrochemical process is a one electron process):

$$Q_{\text{theoretical}} = 0.02 \times 96500 \times 1 / 652.7 = 2.956 \text{ coulomb}$$

$$Q_{\text{experimental}} = 3.5 \text{ coulomb}$$

$$Q_{\text{experimental}}/Q_{\text{theoretical}} = 3.5 / 2.956 = 1.18 \text{ electron}$$

Therefore, the oxidation of the dimers is a one-electron process that corresponds to the oxidation from Fe^{II} to Fe^{III} .

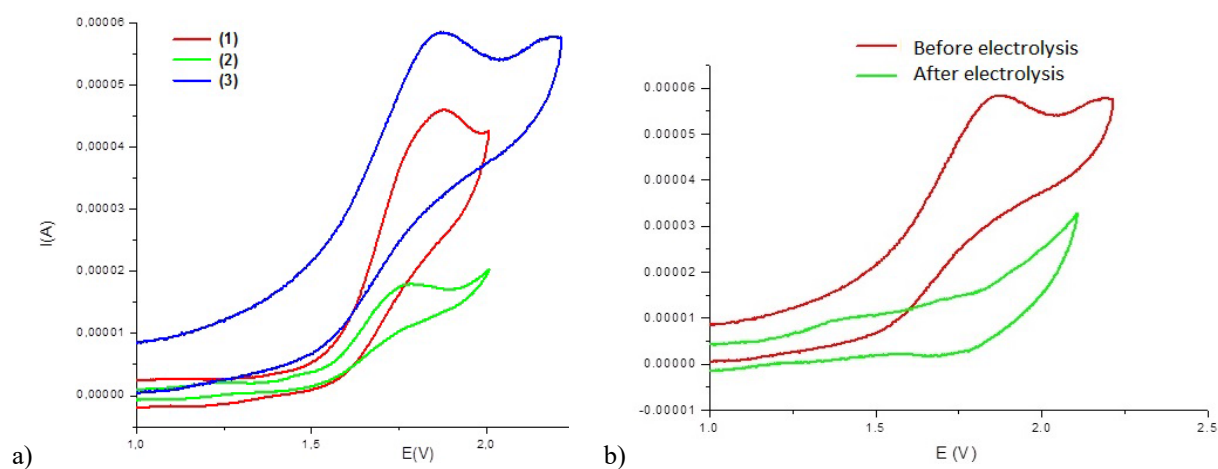


Figure S4. a) Voltammogram of **1-3**, and b) Cyclic voltammogram of **1** in anhydrous CH_2Cl_2 , 0.1 M $(n\text{-Bu}_4\text{N})\text{PF}_6$, 100 mV.

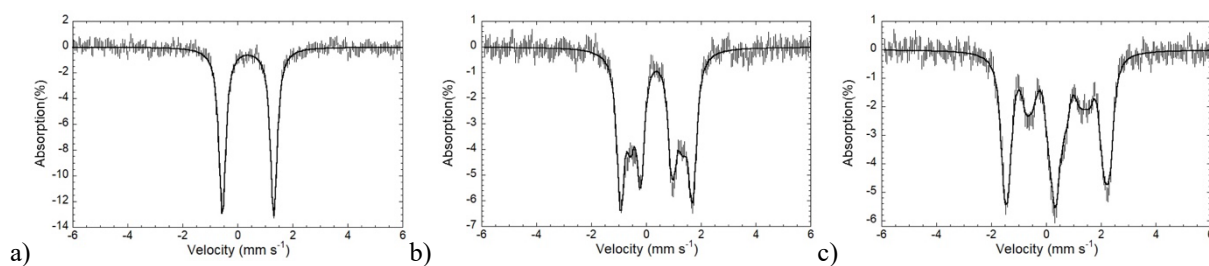


Figure S5. Mössbauer spectra of **1** recorded at 5K under magnetic fields applied parallel to the γ ray of 0.06 T (a), 3 T (b) and 7 T (c) and simulations under the assumption of an $S = 0$ spin. Hashed vertical bars: experimental data, solid line: spectra calculated with the following parameters $\delta = 0.37$ (1) mm s^{-1} and $\Delta E_Q = 1.87$ (3) mm s^{-1} .

The electron paramagnetic resonance (EPR) measurements on the representative complex **1** at helium temperature (parallel and perpendicular modes) showed partial oxidation of this Fe(II)-Fe(II) complex, even though the samples were prepared in an inert atmosphere. Two forms of paramagnetic species were observed. The first corresponds to the oxidation of a Fe(II) ion to Fe(III) (low spin, $S=1/2$, Figure S6b), while the second species exhibits a high integer spin, consistent with the Fe(III)-Fe(III) dimer (Figure S6a).

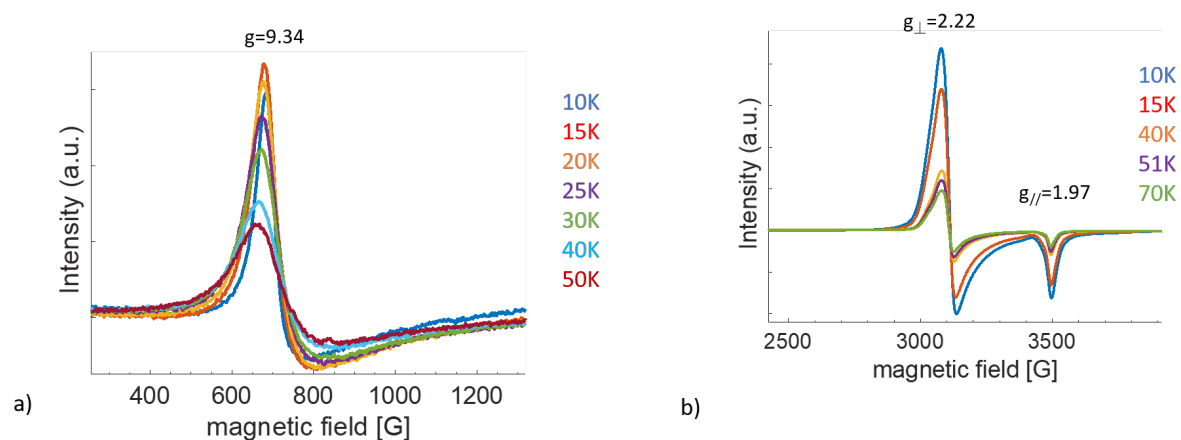


Figure S6: EPR spectra for complex **1** in parallel (a) and perpendicular (b) modes at different temperatures.

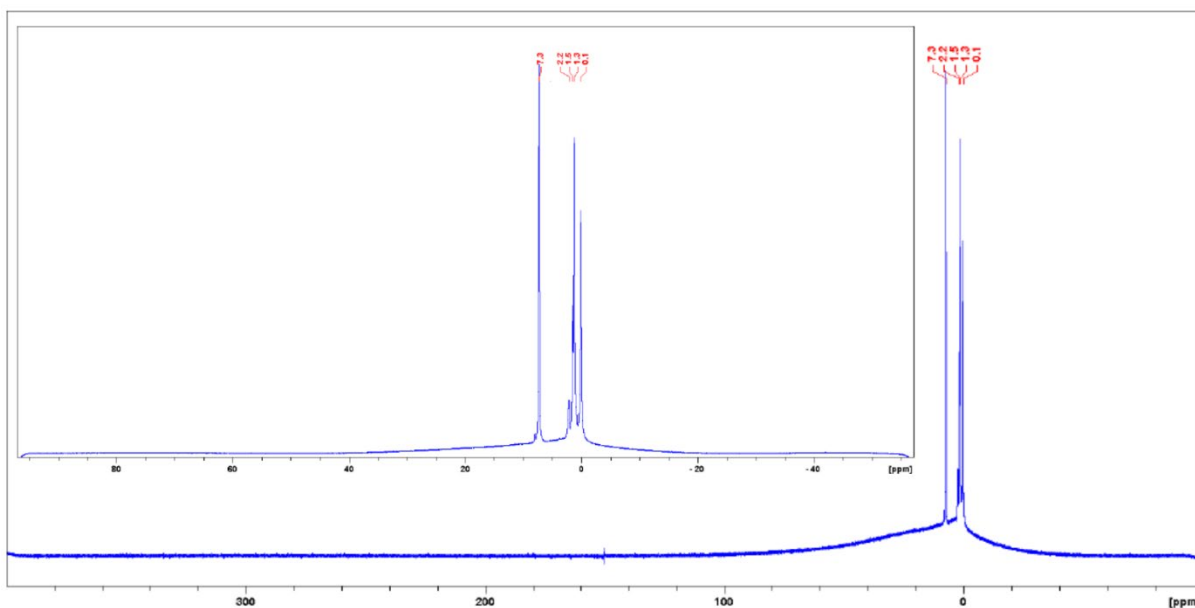


Figure S7: Wide range ^1H NMR spectrum of the Fe-complex **1** in CDCl_3 .

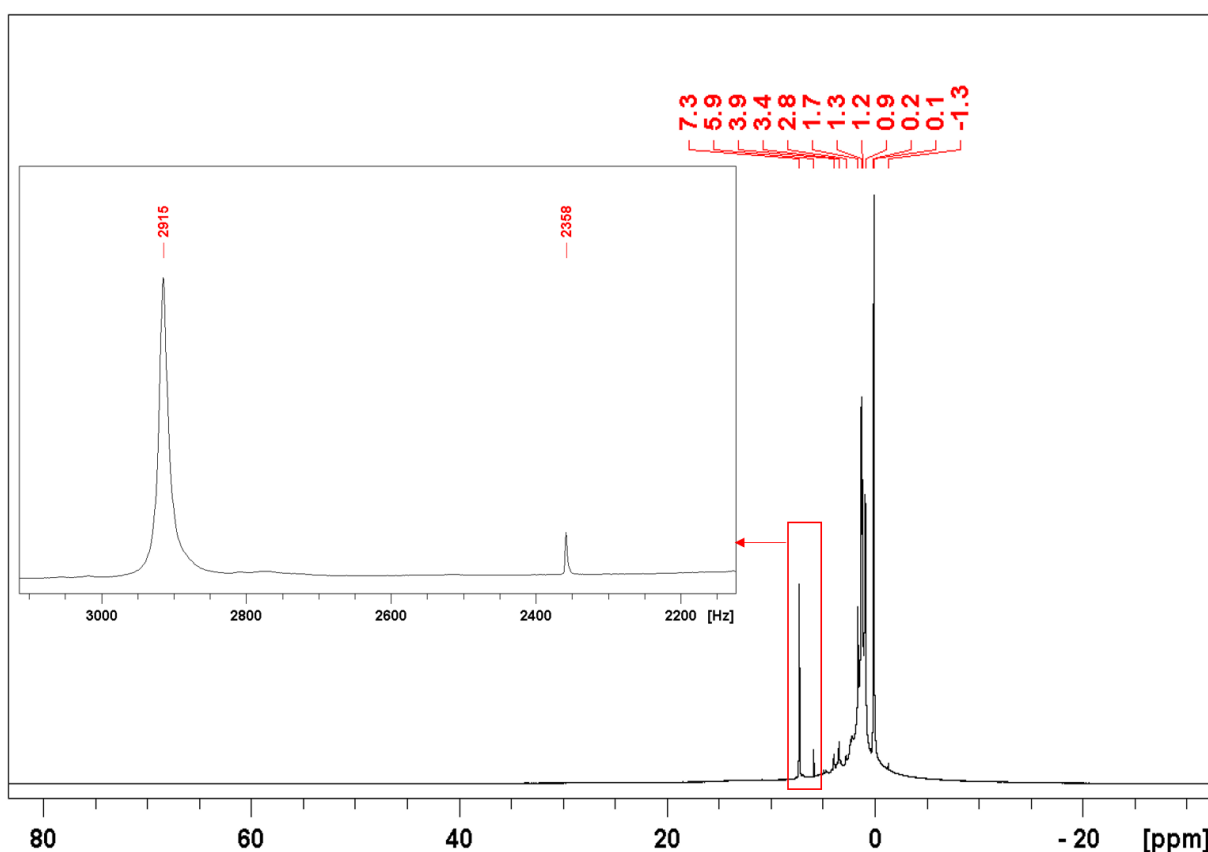


Figure S8: Wide range ^1H NMR spectrum of the Fe-complex **3** in CDCl_3 containing a capillary of the pure solvent within the NMR tube. The inset shows the frequency difference in Hz between the pure solvent resonance and the shifted resonance in the presence of paramagnetic species.

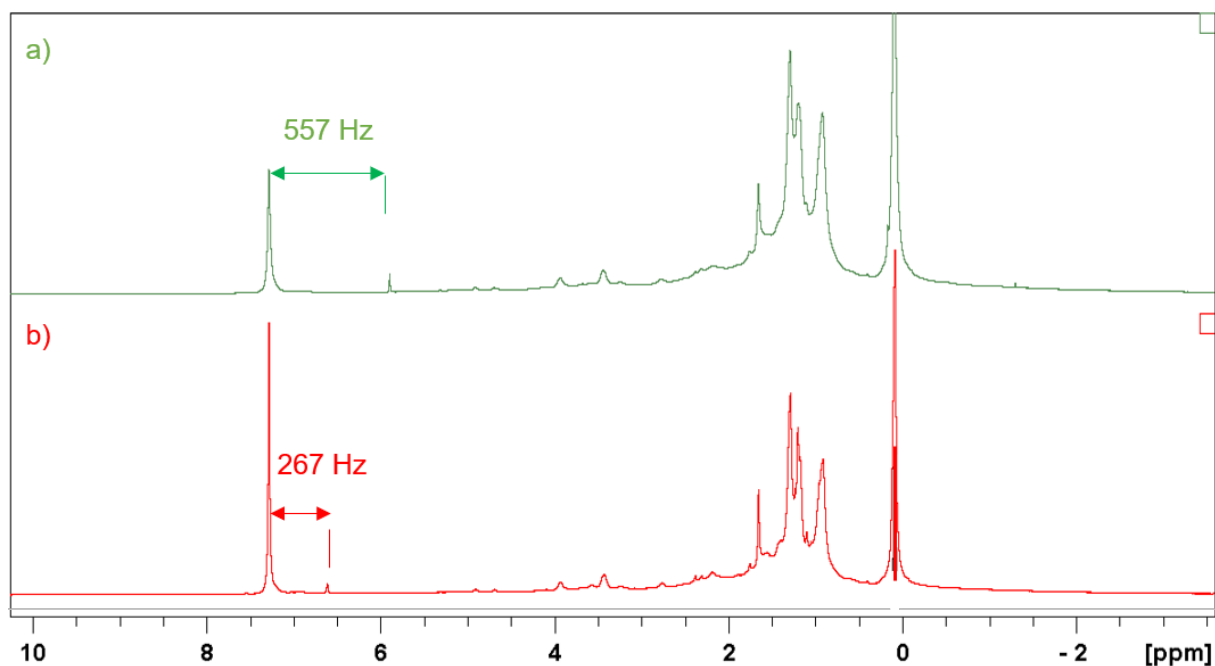


Figure S9: ^1H NMR spectra of the Fe-complex **3** taken in two different concentration in CDCl_3 : a) 1×10^{-4} mol/ml, and b) 0.5×10^{-4} mol/ml. The different concentration of **3** causes change in the frequency difference between the pure solvent resonance (taken in a capillary inside the NMR tube) and the shifted resonance in the presence of the paramagnetic **3**.

Magnetic susceptibility ($\chi_m = 0.00332 \text{ cm}^3/\text{mol}$) and effective magnetic moment ($\mu_{\text{eff}} = 2.81 \mu\text{B}$) of the complex **3** was calculated by Evans method using following equations 2 and 3, respectively:

$$\chi_m = \frac{3 \Delta f}{4\pi F c} \quad (2)$$

$$\mu_{\text{eff}} = \sqrt{8 (\chi_m T)} \quad (3)$$

Where

Δf (frequency difference between the pure and the shifted resonance of the solvent) = 557 Hz

F (magnetic field of NMR instrument) = 400×10^6 (Hz)

c (concentration) = 1×10^{-4} mol/ml

T (Temperature) = 298 K

A lower concentration of **3** (0.5×10^{-4} mol/ml) caused less shifting of the solvent resonance and, therefore, lower frequency difference with the pure solvent resonance (267 Hz, Fig. S9). Using above equations 2 and 3, the magnetic susceptibility ($\chi_m = 0.00318 \text{ cm}^3/\text{mol}$) and effective magnetic moment ($\mu_{\text{eff}} = 2.76 \mu\text{B}$) were calculated.

Table S2. Spin state ordering from single points on the X-ray structure of complex **1** with OLYP, B3LYP and TPSSH for various spin states and configurations: spin densities on each Fe atom (ρ_{Fe}) and total bonding energies E in eV.

Functional	Spin	ρ_{Fe}	E
OLYP	0	0.0	-494.18
	1	1.01	-494.52
B3LYP	0	0.0	-591.29
	1	1.02	-590.63
TPSSH	0	0.0	-571.14
	1	1.01	-571.77

Table S3. Molecular data from geometry optimizations of complex **1** with OLYP and B3LYP for various spin states and configurations: bond lengths in Å, spin density (ρ_{Fe}) on Fe atoms, Mössbauer parameters in mm s^{-1} and total bonding energies E in eV.

Functional	Spin	d(Fe-Fe)	d(Fe-N) _{av}	ρ_{Fe}	δ	ΔE_{Q}	E
OLYP	0	2.25	1.98	+/-1.02			-514.36
	0	2.36	2.02	+/-1.84			-514.09
	0	2.20	1.98	0.0	2.44	0.64	-514.34
	1	2.16	1.99	1.02	1.51	0.60	-514.66
B3LYP	0	2.25	1.95	0.0	2.13	0.42	-610.68
	1	2.14	1.98	1.02	1.51	0.40	-611.17

Table S4. Components of the hyperfine coupling tensor A (MHz), computed with various functionals and basis sets for complex **1**.

	Functional	Basis	A ₁	A ₂	A ₃
ADF	OLYP	TZ2P/QZ4P(Fe, N)	-22.7	-20.4	-7.8
	OPBE	TZ2P/QZ4P(Fe, N)	-23.6	-21.8	-2.2
	PBE	TZ2P/QZ4P(Fe, N)	-18.8	-16.3	2.6
	B3LYP	TZ2P/QZ4P(Fe, N)	-21.8	-20.0	-1.5
Orca	OLYP	Def2-tzvp/CP(PPP)	-27.1	-20.3	-7.2
	OPBE	Fe/IGLO-II N	-31.6	-20.5	-9.4

Cartesian coordinates

a) B3LYP geometry S=1 state.

Fe	-0.821673000	0.682798000	13.362892000
Fe	0.821673000	-0.682798000	13.362892000
N	-1.512272000	-0.250783000	14.966140000
N	-1.164935000	-1.466568000	15.230223000
N	-0.175952000	-1.915145000	14.540915000
N	-1.850165000	-0.517983000	12.177666000
N	-1.225733000	-1.405550000	11.487137000
N	0.031159000	-1.528576000	11.757135000
C	0.070080000	-3.372189000	14.719518000
C	-0.987512000	-4.146366000	13.917009000
C	1.467319000	-3.670462000	14.166774000
C	0.014635000	-3.774170000	16.199593000
C	-2.478716000	0.269520000	15.934745000
C	-1.877917000	0.439972000	17.327897000
C	0.721608000	-2.382300000	10.788368000
C	0.762892000	-1.770778000	9.389741000
C	-3.325577000	-0.530608000	11.977840000
C	-3.877453000	0.769716000	12.570407000
C	-3.689408000	-0.604175000	10.488608000
C	-3.907747000	-1.737003000	12.730564000
H	-0.806243000	-5.221967000	13.974450000
H	-1.980834000	-3.937034000	14.314364000
H	-0.970002000	-3.839513000	12.871791000
H	1.695581000	-4.732022000	14.269697000
H	2.228721000	-3.107047000	14.706984000
H	1.534463000	-3.420220000	13.109015000
H	0.218679000	-4.842074000	16.297065000
H	0.763551000	-3.228191000	16.774192000
H	-0.964090000	-3.565449000	16.626273000
H	-2.812476000	1.235771000	15.557635000
H	-3.356121000	-0.385711000	15.976678000
H	-2.594285000	0.915313000	18.002144000
H	-0.977928000	1.051658000	17.277806000
H	-1.603859000	-0.531100000	17.739555000
H	1.737083000	-2.520528000	11.158677000
H	0.249750000	-3.370573000	10.755696000
H	1.375343000	-2.379241000	8.720456000
H	1.175534000	-0.763816000	9.430413000
H	-0.243940000	-1.707137000	8.978133000
H	-4.957266000	0.821698000	12.426033000
H	-3.682009000	0.829001000	13.639409000
H	-3.431109000	1.638740000	12.085658000
H	-4.774969000	-0.625847000	10.375656000
H	-3.306810000	0.266381000	9.955100000
H	-3.273607000	-1.498411000	10.029462000

H	-4.998464000	-1.740306000	12.672596000
H	-3.608352000	-1.708016000	13.778232000
H	-3.531596000	-2.663210000	12.296002000
N	1.512272000	0.250783000	14.966140000
N	1.164935000	1.466568000	15.230223000
N	0.175952000	1.915145000	14.540915000
N	1.850165000	0.517983000	12.177666000
N	1.225733000	1.405550000	11.487137000
N	-0.031159000	1.528576000	11.757135000
C	-0.070080000	3.372189000	14.719518000
C	0.987512000	4.146366000	13.917009000
C	-1.467319000	3.670462000	14.166774000
C	-0.014635000	3.774170000	16.199593000
C	2.478716000	-0.269520000	15.934745000
C	1.877917000	-0.439972000	17.327897000
C	-0.721608000	2.382300000	10.788368000
C	-0.762892000	1.770778000	9.389741000
C	3.325577000	0.530608000	11.977840000
C	3.877453000	-0.769716000	12.570407000
C	3.689408000	0.604175000	10.488608000
C	3.907747000	1.737003000	12.730564000
H	0.806243000	5.221967000	13.974450000
H	1.980834000	3.937034000	14.314364000
H	0.970002000	3.839513000	12.871791000
H	-1.695581000	4.732022000	14.269697000
H	-2.228721000	3.107047000	14.706984000
H	-1.534463000	3.420220000	13.109015000
H	-0.218679000	4.842074000	16.297065000
H	-0.763551000	3.228191000	16.774192000
H	0.964090000	3.565449000	16.626273000
H	2.812476000	-1.235771000	15.557635000
H	3.356121000	0.385711000	15.976678000
H	2.594285000	-0.915313000	18.002144000
H	0.977928000	-1.051658000	17.277806000
H	1.603859000	0.531100000	17.739555000
H	-1.737083000	2.520528000	11.158677000
H	-0.249750000	3.370573000	10.755696000
H	-1.375343000	2.379241000	8.720456000
H	-1.175534000	0.763816000	9.430413000
H	0.243940000	1.707137000	8.978133000
H	4.957266000	-0.821698000	12.426033000
H	3.682009000	-0.829001000	13.639409000
H	3.431109000	-1.638740000	12.085658000
H	4.774969000	0.625847000	10.375656000
H	3.306810000	-0.266381000	9.955100000
H	3.273607000	1.498411000	10.029462000
H	4.998464000	1.740306000	12.672596000
H	3.608352000	1.708016000	13.778232000
H	3.531596000	2.663210000	12.296002000

b) B3LYP geometry S=0 state.

Fe	-0.868042000	0.719294000	13.360616000
Fe	0.868042000	-0.719294000	13.360616000
N	-1.541192000	-0.243803000	14.908522000
N	-1.162945000	-1.449170000	15.189029000
N	-0.142670000	-1.895888000	14.540068000
N	-1.841161000	-0.483330000	12.174334000
N	-1.212505000	-1.399831000	11.521001000
N	0.040213000	-1.553588000	11.804447000
C	0.122834000	-3.341505000	14.845771000
C	-0.958840000	-4.201484000	14.167855000
C	1.501598000	-3.709169000	14.286216000
C	0.115902000	-3.604729000	16.360292000
C	-2.624668000	0.189097000	15.804891000
C	-2.227896000	0.229684000	17.280449000
C	0.664815000	-2.538303000	10.906712000
C	0.612267000	-2.157318000	9.427062000
C	-3.309195000	-0.479953000	11.861027000
C	-3.918074000	0.812978000	12.414048000
C	-3.562119000	-0.538149000	10.345686000
C	-3.966766000	-1.694899000	12.540312000
H	-0.763018000	-5.262668000	14.337569000
H	-1.940310000	-3.961056000	14.576312000
H	-0.983457000	-4.021191000	13.093381000
H	1.705809000	-4.764338000	14.475504000
H	2.291648000	-3.129417000	14.765152000
H	1.554673000	-3.551131000	13.210854000
H	0.333548000	-4.657801000	16.549294000
H	0.876334000	-3.005333000	16.862475000
H	-0.852138000	-3.366372000	16.795423000
H	-2.925086000	1.185035000	15.480652000
H	-3.491948000	-0.468055000	15.678130000
H	-3.053147000	0.621663000	17.879365000
H	-1.355984000	0.865903000	17.431690000
H	-1.986762000	-0.770205000	17.637902000
H	1.704032000	-2.636230000	11.219505000
H	0.191955000	-3.516601000	11.047689000
H	1.147751000	-2.900278000	8.831479000
H	1.070521000	-1.182706000	9.258992000
H	-0.418518000	-2.114461000	9.078916000
H	-4.992531000	0.824705000	12.222967000
H	-3.774050000	0.897822000	13.489460000
H	-3.488302000	1.691701000	11.932149000
H	-4.636672000	-0.512114000	10.153630000
H	-3.106311000	0.315045000	9.841901000
H	-3.154400000	-1.449433000	9.914500000
H	-5.045277000	-1.690717000	12.366497000
H	-3.789044000	-1.683194000	13.615350000
H	-3.554748000	-2.619487000	12.136744000
N	1.541192000	0.243803000	14.908522000

N	1.162945000	1.449170000	15.189029000
N	0.142670000	1.895888000	14.540068000
N	1.841161000	0.483330000	12.174334000
N	1.212505000	1.399831000	11.521001000
N	-0.040213000	1.553588000	11.804447000
C	-0.122834000	3.341505000	14.845771000
C	0.958840000	4.201484000	14.167855000
C	-1.501598000	3.709169000	14.286216000
C	-0.115902000	3.604729000	16.360292000
C	2.624668000	-0.189097000	15.804891000
C	2.227896000	-0.229684000	17.280449000
C	-0.664815000	2.538303000	10.906712000
C	-0.612267000	2.157318000	9.427062000
C	3.309195000	0.479953000	11.861027000
C	3.918074000	-0.812978000	12.414048000
C	3.562119000	0.538149000	10.345686000
C	3.966766000	1.694899000	12.540312000
H	0.763018000	5.262668000	14.337569000
H	1.940310000	3.961056000	14.576312000
H	0.983457000	4.021191000	13.093381000
H	-1.705809000	4.764338000	14.475504000
H	-2.291648000	3.129417000	14.765152000
H	-1.554673000	3.551131000	13.210854000
H	-0.333548000	4.657801000	16.549294000
H	-0.876334000	3.005333000	16.862475000
H	0.852138000	3.366372000	16.795423000
H	2.925086000	-1.185035000	15.480652000
H	3.491948000	0.468055000	15.678130000
H	3.053147000	-0.621663000	17.879365000
H	1.355984000	-0.865903000	17.431690000
H	1.986762000	0.770205000	17.637902000
H	-1.704032000	2.636230000	11.219505000
H	-0.191955000	3.516601000	11.047689000
H	-1.147751000	2.900278000	8.831479000
H	-1.070521000	1.182706000	9.258992000
H	0.418518000	2.114461000	9.078916000
H	4.992531000	-0.824705000	12.222967000
H	3.774050000	-0.897822000	13.489460000
H	3.488302000	-1.691701000	11.932149000
H	4.636672000	0.512114000	10.153630000
H	3.106311000	-0.315045000	9.841901000
H	3.154400000	1.449433000	9.914500000
H	5.045277000	1.690717000	12.366497000
H	3.789044000	1.683194000	13.615350000
H	3.554748000	2.619487000	12.136744000